



Surface-induced Frustration in Solid State Polymorphic Transition of Native Cellulose Nanocrystals

Reeta Salminen, Niki Baccile, Mehedi Reza, Eero Kontturi

► To cite this version:

Reeta Salminen, Niki Baccile, Mehedi Reza, Eero Kontturi. Surface-induced Frustration in Solid State Polymorphic Transition of Native Cellulose Nanocrystals. *Biomacromolecules*, 2017, 18 (6), pp.1975-1982. 10.1021/acs.biomac.7b00463 . hal-01518291

HAL Id: hal-01518291

<https://hal.sorbonne-universite.fr/hal-01518291>

Submitted on 4 May 2017

HAL is a multi-disciplinary open access archive for the deposit and dissemination of scientific research documents, whether they are published or not. The documents may come from teaching and research institutions in France or abroad, or from public or private research centers.

L'archive ouverte pluridisciplinaire **HAL**, est destinée au dépôt et à la diffusion de documents scientifiques de niveau recherche, publiés ou non, émanant des établissements d'enseignement et de recherche français ou étrangers, des laboratoires publics ou privés.

1
2
3
4
5
6
7 Surface-induced Frustration in Solid State
8
9
10
11 Polymorphic Transition of Native Cellulose
12
13
14
15
16 Nanocrystals
17
18
19
20

21 *Reeta Salminen,^a Niki Baccile,^b Mehedi Reza,^c Eero Kontturi^{*a}*
22

23
24 AUTHOR ADDRESS
25
26

27
28 ^a Department of Bioproducts and Biosystems, School of Chemical Engineering, Aalto
29
30 University, P.O. Box 16300, 00076 Aalto, Finland.
31

32
33 ^b Chimie de la Matière Condensée de Paris, Sorbonne Universités, 75005, Paris, France
34
35

36
37 ^c Department of Applied Physics, P.O. Box 11100, 00076 Aalto, Finland
38
39
40
41

42
43 KEYWORDS: cellulose nanocrystals, host-guest system, image analysis, polymorphic transition,
44
45 surface immobilization
46
47

48
49 ABSTRACT. The presence of an interface generally influences crystallization of polymers from
50
51 melt or from solution. Here, by contrast, we explore the effect of surface immobilization in a direct
52
53 solid state polymorphic transition on individual cellulose nanocrystals (CNCs), extracted from a
54
55 plant-based origin. The conversion from native cellulose I to cellulose III crystal occurred via a
56
57
58
59
60

1
2
3 host-guest inclusion of ethylene diamine inside the crystal. 60% reduction in CNC width (height)
4
5 in atomic force microscopy images suggested that when immobilized on a flat modified silica
6
7 surface, the stresses caused by the inclusion or the subsequent regeneration resulted in exfoliation,
8
9 hypothetically between the van der Waals bonded sheets within the crystal. Virtually no changes
10
11 in dimensions were visible when the polymorphic transition was performed to non-immobilized
12
13 CNCs in bulk dispersion. With reservations and by acknowledging the obvious dissimilarities, the
14
15 exfoliation of cellulose crystal sheets can be viewed as analogous to exfoliation of 2D structures
16
17 like graphene from a van der Waals stacked solid. Here, the detachment is triggered by an inclusion
18
19 of a guest molecule inside a host cellulose crystal and the stresses caused by the firm attachment
20
21 of the CNC on a solid substrate, leading to detachment of molecular sheets or stacks of sheets.
22
23
24
25
26
27

28 INTRODUCTION

29
30
31

32 The possibility of atoms and molecules to organize themselves in multiple different crystalline
33
34 structures, i.e., polymorphism is a common feature of materials with famous cases such as ice,
35
36 silica and carbon.¹⁻⁴ Nearly all crystalline polymers also bear this property. Polymorphism is
37
38 important because the conformation and/or packing of the material affects its physical properties
39
40 such as melting point, conductivity, solubility, or mechanical properties.^{2,4-8} Meanwhile, chemical
41
42 properties are influenced by crystalline packing which often controls the accessibility and
43
44 energetic state of the molecules, thereby affecting their chemical reactivity.^{3,5,9} The extent (degree)
45
46 of crystallinity and the quality of the polymorphs can be tuned in various ways, e.g., by helical
47
48 inducers for polymers.¹⁰⁻¹²
49
50
51
52

53 The presence of an interface can significantly affect the crystalline structure of materials, small
54
55 molecules¹³ and polymers^{14,15} alike. The impact of geometrical confinement in forms of
56
57
58
59
60

droplets,^{16,17} thin films,^{15,18-23} adsorbed structures,^{24,25} composite phases,²⁶⁻²⁸ and blend patterns^{14,29,30} on polymer crystals specifically have been comprehensively investigated. Altogether, the interfacial effect on polymer crystals has far reaching implications in several fields of applications, including drug delivery,³¹ semiconductors,³² and photovoltaics.³³

From the fundamental perspective of interfacial polymer polymorphs, the most common approach is to study crystallization from solution or melt onto a solid surface or perhaps observe the effect of temperature as post treatment that leads to crystallization.¹³⁻¹⁵ Biopolymers, particularly proteins, have also received fair attention in this respect.^{34,35} Furthermore, efforts to elucidate crystallization and melting of monomolecular polymer layers on atomically smooth surfaces have recently undergone an upsurge because of the popular appeal of 2D substrates like graphene.^{36,37} By contrast, actual polymorphic transitions from one crystalline form to another near an interface are generally not investigated and biopolymers present a particularly tricky experimental case for this because of their complex crystallinity. Such solid-state conversions would, however, offer more room for maneuvering the properties of materials that are based on interfacial structures. In this paper, we demonstrate a surface-induced frustration in a polymorphic transition of cellulose, the polysaccharide responsible for the structural scaffold of all plant cells.

In nature, crystalline cellulose occurs always as I_{α} and I_{β} polymorphs. There are two ways of practically altering the crystalline structure: (i) dissolution/regeneration or alkaline swelling leading to cellulose II form and (ii) treatment in liquid ammonia or some diamines like ethylenediamine (EDA) resulting in cellulose III crystals. Of these, the transition to cellulose III is a solid-state conversion: ammonia or diamine molecules enter the otherwise impenetrable cellulose crystal in a host-guest style system, where at formation, the chains slip into the arrangement with altered hydrogen bonding patterns (Figure 1). The major difference between

cellulose III and cellulose I is that in cellulose III the chains are not aligned as flat stacking sheets with van der Waals bonding in between but as conjugated sheets with zig-zagging hydrogen bonding between them.³⁸⁻⁴⁰ This is caused by the primary alcohol rotating into a gauge-trans position from the trans-gauge position during the introduction of the guest molecule into the crystal^{39,41-44} or – as proposed recently – proton hopping from one hydroxyl group to the other.⁴⁵ When the host molecule is removed by rinsing with methanol or ethanol, the gauge-trans position remains in the resulting cellulose III structure (Figure 1).^{42,43} While cellulose I is the strongest and the most inert structure, the increased susceptibility to degradation of cellulose III has elicited suggestions that the polymorphic transition could be used as a pretreatment step when hydrolyzing cellulose into sugars for biofuel production.^{9,38,46}

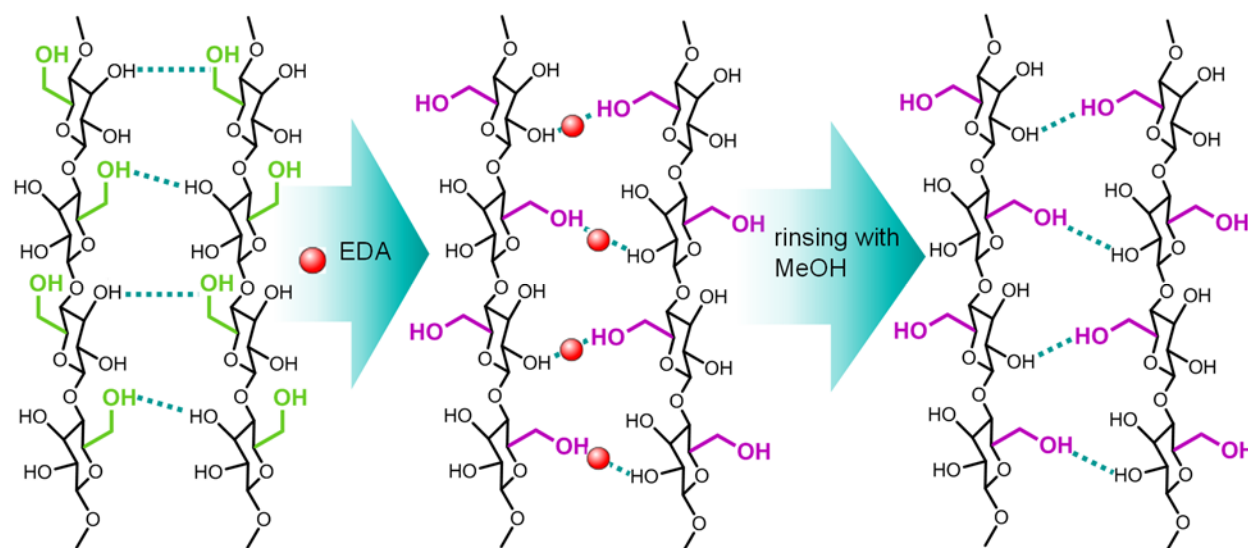


Figure 1. The change in conformation and hydrogen bonding upon EDA-complexation and immersion into methanol.

Here, we utilized the possibility to extract nanosized single crystals of native cellulose I, that is, cellulose nanocrystals (CNCs), directly from plant-based fibers and then closely monitored the morphological changes occurring upon the conversion of cellulose I to cellulose III. This was

performed with two different methods: a) the polymorphic transition cellulose I→III was done in dispersion (Figure 2a), and b) the CNCs were immobilized on a cationized surface, prior to the I→III transition (Figure 2b). It turned out that when CNCs were electrostatically immobilized on a flat substrate, the polymorphic transition was visibly frustrated and the alterations could be ascribed to the breakage in the cellulose crystal. More precisely, the van der Waals bonded sheets in the crystal appeared to be exfoliated upon the frustrated polymorphic transition, which can be seen to resemble the exfoliation of 2D sheets like graphene from van der Waals solids. In this particular instance, however, we have a 1D longitudinal crystal and the exfoliation is triggered by a supramolecular entry of a guest molecule (EDA) in a host cellulose crystal instead of physical shear. The results can be seen as the first step in controlling the supramolecular rearrangements of bio-based polymers directly in solid state.

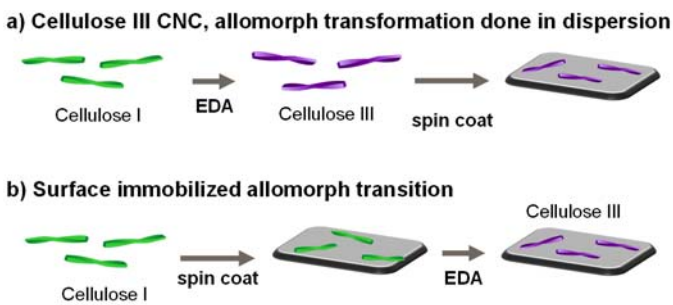


Figure 2. The sample preparation methods: a) The polymorphic transition with ethylenediamine (EDA) is done in dispersion, and then the CNC III is deposited on silicon substrate cationized with 3-aminopropylmethoxysilane (APTS); b) CNC is first deposited on the APTS substrate, and the EDA treatment is performed.

EXPERIMENTAL

Materials. Whatman ashless filter paper was purchased from Whatman GmbH, (Dassel, Germany). Sulfuric acid (H_2SO_4 , 95-97%) ethylenediamine (EDA, $\geq 99.5\%$), sodium hydroxide (NaOH), toluene (anhydrous, 99.8 %), methanol ($\geq 99.8\%$), and (3-aminopropyl)trimethoxysilane (APTS, 97 %) were purchased from Sigma-Aldrich Finland Oy (Helsinki, Finland). Methanol was dried with 3 Å molecular sieves (Fluka) also purchased from Sigma-Aldrich Finland Oy (Helsinki, Finland). Ethanol (Aa grade 99.5% w/v) was purchased from the Altia Corporation (Rajamäki, Finland). Water was purified in a Milli-Q system (Millipore Corporation, resistivity 18.2 MΩ cm). Silicon wafers used as substrates were obtained from Okmetic (Vantaa, Finland), and silicon monoxide coated TEM grids from Science Services GmbH (München, Germany). Nitrogen gas (N_2 ,) was purchased from Oy AGA Ab (Espoo, Finland).

CNC preparation. CNCs were produced from ground Whatman 541 ashless filter paper (15 g) by acid hydrolysis with sulfuric acid (175 ml, 64 w-%) at 45 °C for 45 min, followed by quenching by addition 3 l of MilliQ-water. The CNCs were isolated by centrifugation, followed by purification with dialysis until the conductivity of the dialysis water was $<5\ \mu\text{S}$.⁴⁷ The CNC counter ion was exchanged to Na^+ by adjusting the pH to 7 with 0.1 M NaOH, after which the product was dialysed again and freeze dried.⁴⁸ The CNCs were further purified by Soxhlet extraction with ethanol in order to remove the surface impurities.⁴⁹

Surface cationization of silicon wafers and TEM grids. The silicon wafers were purified before cationization by immersing them into 3 M NaOH-solution for 20 s, followed by careful and excessive rinsing with MilliQ-water.⁵⁰ The wafers were then dried with N_2 and placed into ozonator (Bioforce Nanosciences UV.TC.EU.003) for 15 minutes followed by rinsing with water and drying with N_2 . The cationization of silicon wafers with APTS was done by immersing the

cleaned wafers into 1 % (v/v) APTS toluene solution for 40 minutes, rinsed with approximately 50 ml of toluene and dried in an oven for 30 minutes at 60 °C.⁵¹ The TEM grids were cationized with the same method, omitting the purification steps.

Immobilization of CNCs on silicon wafers and TEM grids. The inherently anionic CNCs were then immobilized on the APTS surface (Figure 3) by spin coating (4000 rpm, 2200 rpm s⁻¹) with WS-650SX-6NPP/LITE spin coater (Laurell Technologies Corporation, North Wales, PA, USA) and were cured in oven for 10 minutes at 80 °C. The low CNC concentration in the dispersion used (10 mg dm⁻³) formed submonolayers on the APTS surface. The cellulose III CNC submonolayers were also produced on APTS surfaces, but with a higher dispersion concentration (500 mg dm⁻³) due to a steep decrease in charge during the polymorphic transition.

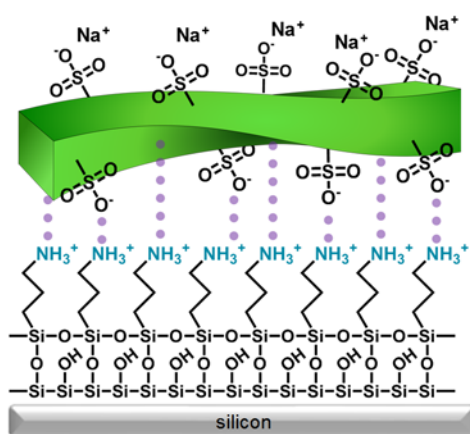


Figure 3. Immobilization of CNC on the cationic APTS surface. The purple dotted lines represent the electrostatic interactions between the cationized surface and the anionic CNC. The scheme is not in scale.

TEM samples were prepared by the CNCs were adsorbed on the cationized TEM grids (10 µl, 10 mg dm⁻³), the excess rinsed with milliQ-water, and the excess water blotted carefully with filterpaper. The samples were allowed to air dry before the EDA treatment. For reference samples without the EDA treatment were also imaged.

The polymorph transition. Cellulose I was transformed into cellulose III by dispersing the CNCs into 75 % aqueous ethylenediamine (EDA) solution for 5 h at 35 °C, after which the EDA solution was decanted and the CNCs immersed in anhydrous methanol.⁴³ The methanol was decanted off and replaced with fresh anhydrous methanol. The washing step was repeated several times. The CNCs were then air dried.

The polymorph transition of immobilized cellulose I to cellulose III were performed on the submonolayers of CNC. In these samples the EDA reaction time was 3 h in order to protect the presumably delicate cationized surface.

Conductometric titration. Dried particles (0.2 g) were dispersed to 100 ml degassed water and 0.2 ml of 0.5 M NaCl added. The CNC was then protonated with 0.1 M HCl, and was stirred for 30 minutes. The dispersion was then titrated with 0.1 M NaOH-solution at rate 0.10 ml min⁻¹ adjusted by 751 GPD Titrino, Metrohm (Herisan, Switzerland). The charge content was determined from the conductivity curve obtained with Metrohm 712 conductometer (Herisan, Switzerland) where only one charged species was detected (sulfate groups). For untreated cellulose I CNCs, the charge was determined as 0.45 mmol g⁻¹ and for the cellulose III CNC, treated with EDA in dispersion, the amount of charged groups was 0.04 mmol g⁻¹.

Atomic Force Microscopy (AFM). The submonolayers were imaged as presented in Figure 2: the cellulose III surfaces as they were and the surface immobilized transition samples before and after the EDA treatment. The imaging was performed with AFM MultiMode 8 scanning probe microscope from Bruker AXS Inc. (Madison, WI, USA) with an E scanner in tapping mode. The cantilevers used were NSC15/AIBS silicon cantilevers from Ultrasharp μ masch (Tallinn, Estonia). The particle dimensions were obtained using SPIP 6.0.6 particle analysis. The width of the particles was determined from the height scale to overcome the error caused by the AFM tip

convolution. For sufficient statistical sampling 10 samples of each CNC type was imaged from 4 different spots.

Transmission electron microscopy (TEM). Cellulose I CNC and cellulose III CNC were imaged with a field-emission cryo-Transmission Electron Microscope (cryo-TEM, JEOL JEM-3200FSC). The sample temperature was maintained at -187 °C during the imaging. The images were taken in bright-field mode using zero-loss energy filtering (Omega type) with a slit width of 20 eV. Micrographs were recorded with a Gatan Ultrascan 4000 CCD camera and using Gatan DigitalMicrograph software (Gatan, Pleasanton, CA, USA).

Solid state NMR. ^{13}C solid-state Cross-Polarization (CP) Magic Angle Spinning (MAS) NMR experiments have been acquired on a Bruker Avance 300 MHz (7 T) spectrometer using 7 mm zirconia rotor spinning at a MAS frequency of $\nu_{\text{MAS}} = 5$ kHz. The contact time is set to 2 ms, the recycling delay is set to 5 s and 320 transients have been used. CP is commonly used for its high sensitivity, however, CP is also known not to be quantitative as the peak relative intensities depend on the choice of the contact time. For this reason, we have also performed single pulse (SP) experiments using a classical high power heteronuclear decoupling pulse sequence, the disadvantage of SP being the poor signal-to-noise ratio. For these experiments, the recycle delay is set to 60 s and the number of transients to 120. Chemical shifts were referenced relative to tetramethylsilane (TMS; $\delta = 0$ ppm). Deconvolution is initially performed on the CP-MAS Cellulose I spectrum for its high signal-to-noise ratio and then used to deconvolute the Cellulose III CP-MAS spectrum simply by letting the intensity vary. The SP-MAS spectra are then deconvoluted using the data from CP-MAS and only intensity is allowed to vary.

RESULTS AND DISCUSSION

The polymorphic transition of CNCs in dispersion (Figure 2a) was followed by solid state nuclear magnetic resonance spectroscopy (^{13}C NMR). The conversion from cellulose I to III was performed by first preparing the EDA-cellulose complex from freeze dried CNCs and rinsing the EDA away with methanol – altogether an established procedure for cellulosic fibers⁴³ but not previously reported for CNCs. This change to cellulose III in bulk dispersion was determined with ^{13}C MAS NMR both using Cross Polarization (CP) (Figure S3) and single pulse (SP) (Figure 4 and S2), the latter being used as a complement for CP experiments, more sensitive but known to be not quantitative. Cellulose I and cellulose III can be identified by the difference in chemical shift of the C6 peak, resonating at about 65 ppm and 63 ppm (Table S1), respectively, for cellulose I and cellulose III.^{39,52,53} Before phase change, cellulose I is characterized by two C6 resonances (Figure 4), at 65.66 ppm and 63.04 ppm, respectively indicating the bulk and surface contribution of the CNCs, as suggested by Brinkmann et al.⁵⁴ After phase change, the bulk cellulose I contribution at 65.66 ppm is reduced by a factor 2.5 after CP, a value which is confirmed by the quantitative SP experiments (2.3) (Table S1). Meanwhile, the increase in the cellulose III resonance at 63.04 ppm is also estimated to a factor of 2.5. If one neglects, to a first approximation, the surface contribution of cellulose I before and after the phase change, one can reasonably estimate that cellulose III represents, after phase change, an average of $75 \pm 4\%$ of the material, whereas the respective values for CP and SP experiments are 71% and 79% (see Supporting Information). More than just one EDA treatment would have undoubtedly increased the extent of cellulose III conversion, but we opted for a single treatment because EDA reduced the number of sulfate groups on the CNC surface and further exposures would have caused more problems in the eventual immobilization of CNCs, based on the attraction between sulfates and the APTS surface.

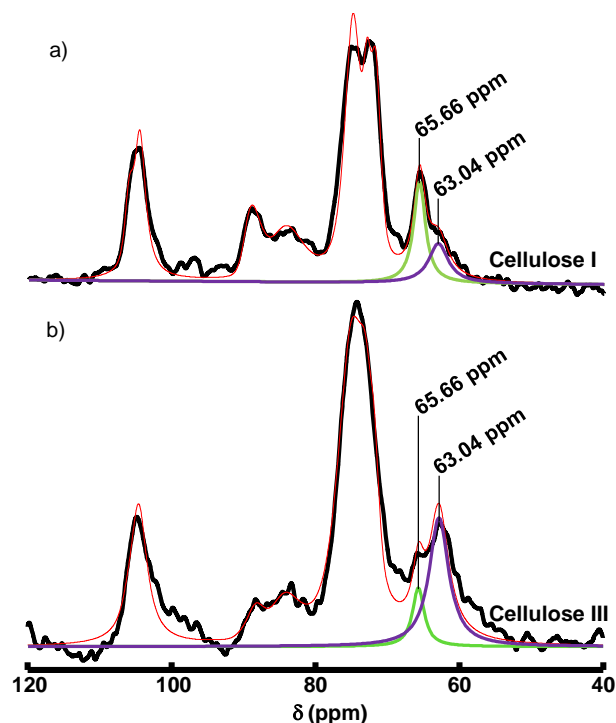


Figure 4. SP-MAS ^{13}C -NMR spectra of a) cellulose I CNC and b) cellulose III CNC with peak fits for C6-chemical shift. The purple curve is the peak fit to peak 63.04 ppm (cellulose III, and disordered cellulose on the crystal surface) and green to 65.66 ppm (cellulose I). The red curve is the peak fit sum. Full peak fit spectra can be found from Supporting Information (Figure S2).

The morphology of the CNCs upon cellulose I to III conversion in dispersion was followed by AFM (Figure 5) and particle size analysis from the respective images (Figure 6, Figure S1 and Table S2). The CNCs were deposited on a silicon surface that was cationized with 3-aminopropylmethoxysilane (APTS). As the CNC surfaces are dotted with anionic sulfate groups, the cationic APTS surface enabled nice separation of the CNCs, allowing a close examination of the crystals individually. However, cellulose III CNCs produced in dispersion required a higher dispersion concentration to yield an examinable submonolayer (Figure S1) because of a decreased surface charge from 0.4 mmol g^{-1} to 0.04 mmol g^{-1} as shown by conductometric titration. A similar reduction in surface charge has been observed when CNCs have been treated with alkaline, and

1
2
3 because EDA is highly alkaline, this was expected.^{55,56} Dimensional analysis from AFM images
4 (Figure 6a) of the original cellulose I CNCs gave average dimensions length of 114 nm and width
5 of 4.5 nm (Table S2). CNC widths were actually deduced from CNC height because of the AFM
6 tip deconvolution and because we deemed this as a more appropriate way of analyzing the width
7 of a single cellulose crystal in a CNC. It is generally agreed that most CNCs are actually flat, lateral
8 aggregates of 2-4 crystallites.⁵⁷ When deposited for AFM analysis, the aggregates lie flat on the
9 substrate and the AFM height analysis yields a value for a single crystal in the flat aggregate.⁵⁷
10 Any compaction of the stiff cellulose crystal upon deposition to a solid substrate is unlikely and
11 has never been reported. Contrary to AFM, TEM allows only the lateral dimensions to be analyzed
12 and the width in the TEM images obviously represents the whole aggregate,⁵⁷ which is also
13 consistent with our TEM results (Figure S4). In conclusion, AFM height analysis from CNC
14 aggregates yields a realistic figure for a single cellulose crystal and this value (4.5 nm, Table S2)
15 is consistent with the values for single crystals in cotton CNCs also in the study that reported the
16 aggregates in the first place.⁵⁷
17
18
19
20
21
22
23
24
25
26
27
28
29
30
31
32
33
34
35

36 The width of dispersion method cellulose III crystals in CNCs was very similar to that of the
37 original cellulose I crystals: width 5.2 nm and length 138.0 nm (Figure 5b and 6b, Table S2).
38 Transmission Electron Microscopy (TEM) of cellulose I and III CNCs supported the observation
39 that the crystal dimensions remained fairly unchanged before and after the polymorph transition
40 (Figure S4), although the TEM analysis yields the width for the whole aggregate in a CNC. Judging
41 from the unit cell parameters, the crystal dimensions of cellulose I and III should be similar to each
42 other and, therefore, the close resemblance of the CNC dimensions is no surprise.³⁸ In contrast,
43 when polymorphic transition was performed by strong aqueous NaOH solution on individual
44 CNCs to cellulose II crystalline form where the morphology is changed completely from rod-like
45
46
47
48
49
50
51
52
53
54
55
56
57
58
59
60

1
2
3 to spherical.⁵⁵ The contrast underlines the fundamental differences between the polymorphic
4 transitions of cellulose I into cellulose II and cellulose III.
5
6

7
8 When the lattice transition was performed on CNCs immobilized on an APTS treated silicon
9 surface (Figure 2b), the width of the crystals in cellulose III CNCs dropped to half of their original
10 size, 2.1 nm, whereas their average length did not change (Figure 5c and 6c, Table S2). Clearly,
11 some of the CNCs were detached from the surface, possibly due to the decreased electrostatic
12 attraction because of the cleavage of sulfate groups during exposure to EDA since the dissociation
13 of the sulfates should not be affected as EDA is highly alkaline. Therefore, one could question
14 whether the decreased width is just a statistical illusion of thicker crystals being detached and
15 thinner ones remaining on the surface. The number of CNCs on a sampled surface area does indeed
16 decrease from over 2600 (Table S2) to less than 800, but the initial amount of the CNCs thinner
17 than 2 nm (12 out of 2694) was not enough to explain the thin CNCs (330 out of 726) observed
18 after the EDA treatment as seen from Figure 6. The EDA treatment for the immobilized CNCs
19 was also performed by rinsing with water instead of methanol afterward (Figure 5d), which
20 reportedly does not result in a change in the crystal lattice, i.e., the EDA-cellulose complex reverts
21 back to a somewhat more disordered cellulose I structure.^{42,43} However, the results of water rinsing
22 experiments were that the crystals thinned to an average width of 1.8 nm (Table S2), i.e., the same
23 as when rinsed with methanol. In conclusion, the crystal thinning with CNCs appears to occur
24 during EDA swelling or regeneration upon its removal and it occurs exclusively to the surface
25 immobilized CNCs because no thinning was observed for the CNCs treated in bulk dispersion
26 (Figures 5 and 6).
27
28
29
30
31
32
33
34
35
36
37
38
39
40
41
42
43
44
45
46
47
48
49
50
51
52

53 Synchrotron-enhanced grazing incidence wide angle x-ray scattering (GI-WAXS) was
54 attempted to corroborate the decrease in crystal width and to elucidate the polymorph transition,
55
56
57
58
59
60

but the amount of material was too small in the submonolayers to yield a meaningful diffraction pattern.

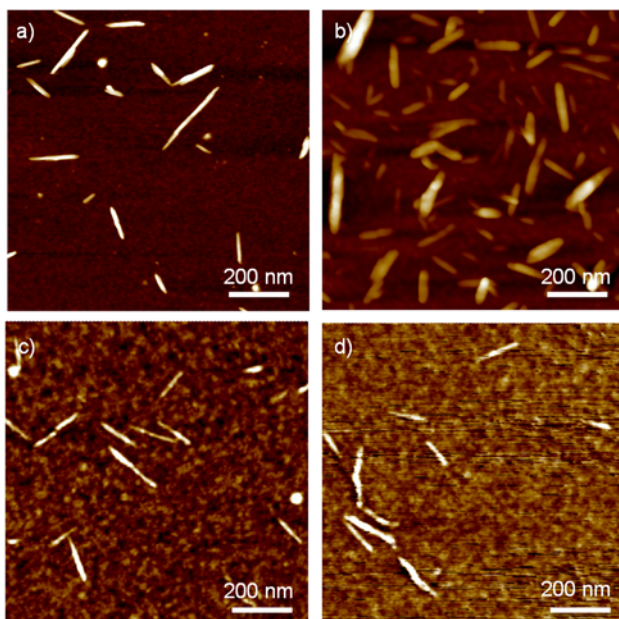


Figure 5. $1 \times 1 \mu\text{m}^2$ AFM height images: a) CNC b) CNC III, dispersion method c) CNC III, immobilized on the substrate before EDA-treated, rinsed with methanol d) CNC III, immobilized while EDA-treated, rinsed with water. Spherical objects present in a), c) and d) are impurities caused by APTS.

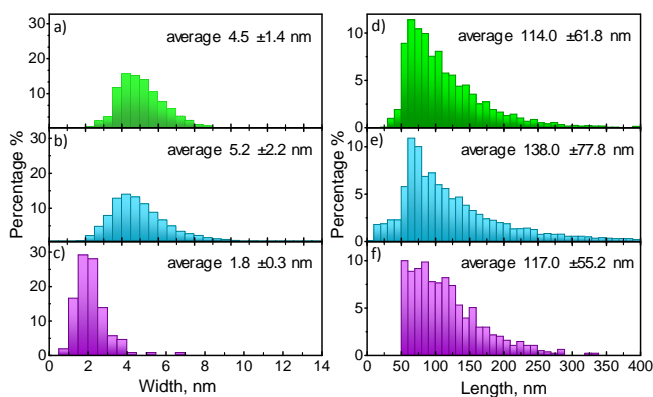


Figure 6. Dimensional distributions as determined from the AFM images. The width distributions are presented on the left column for a) cellulose I CNC, b) cellulose III CNC produced in dispersion, and c) cellulose III CNC produced while immobilized on substrate. The length distributions are on the right side for d) cellulose I CNC, e) cellulose III CNC produced in dispersion, and f) cellulose III CNC produced while immobilized on substrate. The width was determined as the height of CNCs from the substrate surface to omit the tip convolution. The APTS impurities were omitted from the particle analysis.

When the immobilization experiment was repeated with APTS-modified silica-based TEM grids the crystal thinning upon polymorph conversion was not as obvious as with AFM (Figure S5). The APTS-coating on TEM-grids behaved differently than the APTS-coating on silica wafer, i.e., the CNC separation was not as efficient as on a smooth silica surface (Figure S5a). As previously discussed, TEM shows the aggregate size in a CNC rather than the width of an individual crystallite and this is also evident for both the cellulose III CNCs prepared in dispersion (Figure S5b) and the ones prepared immobilized on the surface (Figure S5b). As a result, overall CNC widths for the cellulose I CNC and cellulose III CNC prepared in dispersion were larger, 15.2 nm and 18.5 nm (Figure S5a and S5b), compared to the crystal widths determined by AFM height analysis, 4.5 nm and 5.2 nm, respectively. Similarly, the EDA treated immobilized CNCs show up as aggregates in TEM images (Figure S5c). However, these CNC aggregates are slightly thinner as 12.9 nm (Figure S5c) than the reference immobilized cellulose I CNC aggregates (15.2 nm). All in all, although the TEM experiments suggested that CNC thinning upon polymorphic transition does occur, the aggregation impeded making quantitative conclusions on the TEM images and hence the AFM results were regarded as statistically more reliable because the height analysis of the flat aggregates is able to reveal the alterations in the width of an individual crystal in a CNCs.

As stated before, surface-induced polymer crystallization from solution or from melt is a common phenomenon but an interfacial effect in a solid state polymorphic transition has rarely been explored. The decrease in the CNC width observed particularly with AFM can be hypothetically explained by exfoliation of the outer layers of the crystals during the EDA treatment of the CNCs immobilized on a surface. In the native CNC, i.e., in a cellulose I crystal, the hydrogen bonded cellulose chains form molecularly thin sheets which are stacked on top of each other by van der Waals bonds (Figure 7).⁵⁸ When EDA swells the crystal by host-guest inclusion and the crystal is subjected to stress because of the immobilization, and we can speculate that the weaker van der Waals bonds would be more susceptible to cleavage than the stronger hydrogen bonds which are rearranged in the polymorphic transition process. The flat aggregates of CNCs could be disintegrated as well, but this would not explain the width (height) decrease observed with AFM. To better illustrate the case, we collected several high-resolution AFM images of individual immobilized CNCs that had undergone cellulose I to III conversion (Figure 8). The proposed exfoliation is especially visible in Figures 8b, 8d and 8e, where the immobilized CNC appears to have been cleaved in the longitudinal direction, with a thinner crystallite layer still attached to the CNC. Such defibrillation during a polymorphic transition has been previously reported for large cellulose microfibrils in *Valonia* alga but the authors speculated that the breakage could have been caused by the large size of the crystal, allegedly composed of smaller elementary units.^{44,52} Moreover, the morphological alterations were not induced by the presence of an interface like in our case and the crystal thinning did not appear systematic. It appears that the binding to a surface prior to the host-guest type of entry by EDA into the crystallite causes strain in the lattice (Figure 7). Furthermore, the cellulose chains closest to the cationized surface are hindered from tilting in the cellulose-EDA complex (Figure 7, phases 1 and 2) causing the upper layers to become

1
2
3 frustrated, and hence prone to break from the lattice and cause thinning. The fact that this
4
5 phenomenon of exfoliation was also present in the experiments on immobilized CNCs rinsed with
6
7 water (Figure 5d) strongly suggests that it occurs during the EDA complexation or indeed during
8
9 the regeneration to either cellulose III or cellulose I upon removal of EDA. In fact, the regeneration
10
11 can be a more plausible phase to enable exfoliation: the EDA actually plasticizes the swollen
12
13 crystal while the crystal shrinks during regeneration, rendering it more susceptible to frustration
14
15 by the underlying interfacial strain. Whatever the mechanisms for the exfoliation may be, the
16
17 presence of constraints imposed by the surface immobilization are still crucial for the exfoliation
18
19 to take place since no such phenomenon was observed in cellulose III CNCs produced in a bulk
20
21 dispersion (Figure 5).
22
23
24
25
26
27
28
29
30
31
32
33
34
35
36
37
38
39
40
41
42
43
44
45
46
47
48
49
50
51
52
53
54
55
56
57
58
59
60

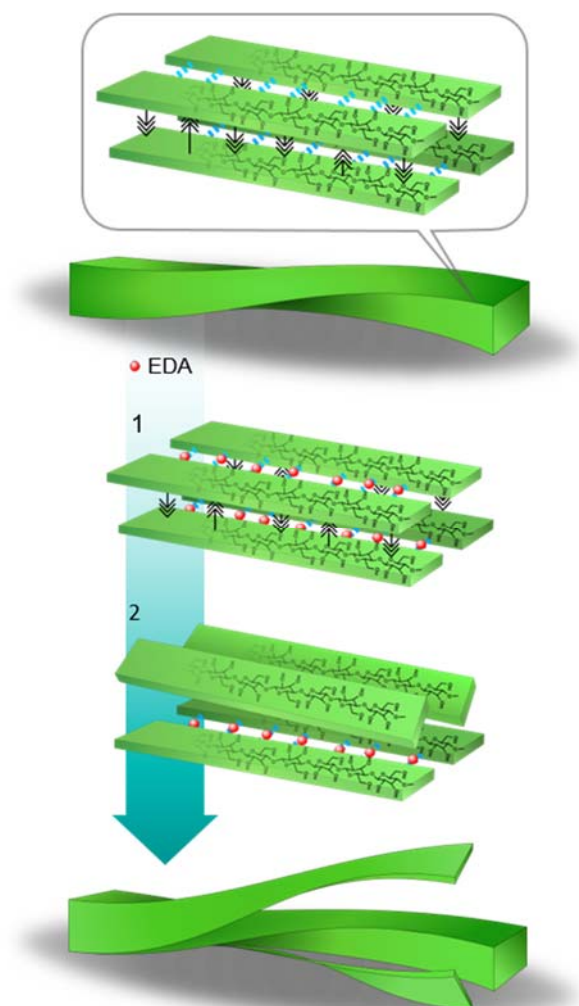


Figure 7. A schematic presentation of cellulose chains in a CNC. When EDA is introduced to for the host-guest complex (1) the lower chains are prevented to tilt (2) hypothetically causing exfoliation of layers of the CNC.

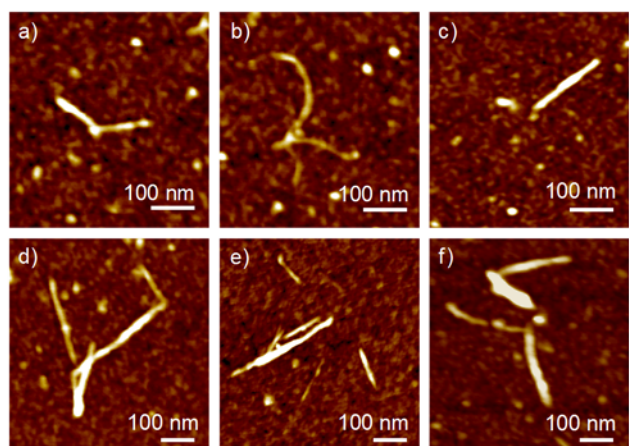


Figure 8. A collection of high resolution AFM height images of broken CNCs caused by EDA-complex formation while immobilized on APTS-modified substrate. Representative height profiles of these CNCs are presented in the Supporting Information (Figure S6)

In some ways, the structure of the cellulose crystal and the exfoliation of the layers is reminiscent of van der Waals solids and the exfoliation of 2D structures such as graphene or MoS_2 ,^{59,60} only one of the two lateral dimensions here is just a few molecular layers wide. Indeed, the exfoliation of graphene from graphite is enabled by the individualization of covalently bonded carbon sheets that are van der Waals bonded to one another just like the sheets formed by strong hydrogen bonding in cellulose hypothetically may be detached from one another by EDA inclusion because there is weaker van der Waals bonding between them.⁶¹ Even covalent breakage of polymer chains by interfacial stress in so-called fatal adsorption has been reported, indicating that the forces can be truly significant upon surface induced frustration.⁶² Furthermore, physical exfoliation of the van der Waals bonded sheets in a cellulose I crystal has been claimed before by a means of high intensity sonication,⁶³ further strengthening our hypothesis of selective cleavage of cellulose crystal sheets by EDA. We must emphasize that the attribution of the specific site of exfoliation to the van der Waals bonded sheets is entirely speculative. Further studies in, e.g., molecular

dynamics simulations are required to further illuminate the case. If the specific site for exfoliation can be verified, this may be useful even in the design of novel cellulose solvents which always require an effective agent to break both the hydrogen bond and the van der Waals bond networks.

CONCLUSION

When the movement of the CNCs was restricted by electrostatic interactions with the substrate during the polymorphic transition from cellulose I to cellulose III, the average width of individual crystals in CNCs decreased from 4.5 nm to 2.1 nm as determined by height analysis from AFM images. However, when transition was performed by EDA treatment to CNCs in dispersion, no changes were observed in the crystal dimensions of CNCs, which was in line with the similar unit cell dimensions of both polymorphs. We hypothesize that the immobilization on the substrate causes frustration in the crystal lattice during the polymorphic transition. The frustration causes the lattice to break, which is observed as a decreased thickness in CNC.

An important note is that the thinning seems to happen during the EDA complex formation or lattice regeneration, since when the immobilized CNCs were rinsed with water after the EDA treatment, the crystal width decreased similarly as when rinsed with methanol. This supports the frustration hypothesis as a reason for the exfoliation, since the frustration would happen only in the presence of the surface-CNC interactions at lattice change either during complexation with EDA or upon regeneration to cellulose I or cellulose III.

In essence, this study reports the chemical exfoliation of molecularly thin structures from a biologically derived crystalline nanomaterial, aided by deliberately built interfacial stress. It may serve as a starting point for similar efforts that can potentially lead to a new family of ultrathin biological materials.

1
2
3
4
5
6
7
8
9
10
11
12
13
14
15
16
17
18
19
20
21
22
23
24
25
26
27
28
29
30
31
32
33
34
35
36
37
38
39
40
41
42
43
44
45
46
47
48
49
50
51
52
53
54
55
56
57
58
59
60

ASSOCIATED CONTENT

The following files are available free of charge.

Supporting Information. NMR fitting procedures, TEM images, and further AFM images with height profiles and dimensional data.

AUTHOR INFORMATION

Corresponding Author

eero.kontturi@aalto.fi

Funding Sources

This research is funded by the Academy of Finland (Project 259500).

ACKNOWLEDGMENT

Dr. Jessie Peyre (UPMC, France) is acknowledged for measuring the charge of untreated CNCs.

ABBREVIATIONS

CNC, cellulose nanocrystal; CP-MAS ^{13}C -NMR, cross-polarization magic angle spin ^{13}C -nuclear magnetic resonance; SP-MAS, single pulse magic angel spin; AFM, atomic force microscopy; TEM, transmission electron microscopy; APTS, 3-aminopropyltrimethoxysilane; EDA, ethylenediamine

REFERENCES

1. Gaffney, E. S.; Matson, D. L. Water ice polymorphs and their significance on planetary surfaces. *Icarus* **1980**, *44*, 511-519.
2. Keskar, N. R.; Chelikowsky, J. R. Structural properties of nine silica polymorphs. *Phys. Rev. B* **1992**, *46*, 1-13.
3. Dubrovinsky, L. S.; Dubrovinskaia, N. A.; Prakapenka, V.; Seifert, F.; Langenhorst, F.; Dmitriev, V.; Weber, H.; Le Bihan, T. A class of new high-pressure silica polymorphs. *Phys. Earth Planet. Inter.* **2004**, *143–144*, 231-240.
4. Hazen, R. M.; Downs, R. T.; Jones, A. P.; Kah, L. Carbon Mineralogy and Crystal Chemistry. *Rev. Mineral. Geochem.* **2013**, *75*, 7-46.
5. Mercury, L.; Vieillard, P.; Tardy, Y. Thermodynamics of ice polymorphs and ‘ice-like’ water in hydrates and hydroxides. *Appl. Geochem.* **2001**, *16*, 161-181.
6. Tchijov, V. Heat capacity of high-pressure ice polymorphs. *Journal of Physics and Chemistry of Solids* **2004**, *65*, 851-854.
7. Li, Q.; Ma, Y.; Oganov, A. R.; Wang, H.; Wang, H.; Xu, Y.; Cui, T.; Mao, H.; Zou, G. Superhard Monoclinic Polymorph of Carbon. *Phys. Rev. Lett.* **2009**, *102*, 175506-1-175506-4.
8. Miller, E. D.; Nesting, D. C.; Badding, J. V. Quenchable Transparent Phase of Carbon. *Chem. Mater.* **1997**, *9*, 18-22.
9. Igarashi, K.; Wada, M.; Samejima, M. Activation of crystalline cellulose to cellulose III_I results in efficient hydrolysis by cellobiohydrolase. *FEBS J.* **2007**, *274*, 1785-1792.

- 1
2
3 10. Kawauchi, T.; Kumaki, J.; Kitaura, A.; Okoshi, K.; Kusanagi, H.; Kobayashi, K.; Sugai, T.;
4
5
6 Shinohara, H.; Yashima, E. Encapsulation of Fullerenes in a Helical PMMA Cavity Leading to a
7
8 Robust Processable Complex with a Macromolecular Helicity Memory. *Angew. Chem.* **2007**,
9
10 *120*, 525-529.
11
12
13 11. Yashima, E.; Matsushima, T.; Okamoto, Y. Poly((4-carboxyphenyl)acetylene) as a Probe for
14
15 Chirality Assignment of Amines by Circular Dichroism. *J. Am. Chem. Soc.* **1995**, *117*, 11596-
16
17 11597.
18
19
20 12. Inai, Y.; Tagawa, K.; Takasu, A.; Hirabayashi, T.; Oshikawa, T.; Yamashita, M. Induction of
21
22 One-Handed Helical Screw Sense in Achiral Peptide through the Domino Effect Based on
23
24 Interacting Its N-Terminal Amino Group with Chiral Carboxylic Acid. *J. Am. Chem. Soc.* **2000**,
25
26 *122*, 11731-11732.
27
28
29 13. Jones, A. O. F.; Chattopadhyay, B.; Geerts, Y. H.; Resel, R. Substrate-Induced and Thin-
30
31 Film Phases: Polymorphism of Organic Materials on Surfaces. *Adv. Funct. Mater.* **2016**, *26*,
32
33 2233-2255.
34
35
36 14. Michell, R. M.; Müller, A. J. Confined crystallization of polymeric materials. *Prog. Polym.*
37
38 *Sci.* **2016**, *54-55*, 183-213.
39
40
41 15. Li, H.; Yan, S. Surface-Induced Polymer Crystallization and the Resultant Structures and
42
43 Morphologies. *Macromolecules* **2011**, *44*, 417-428.
44
45
46 16. Carvalho, J. L.; Dainoki-Veress, K. Homogeneous Bulk, Surface, and Edge Nucleation in
47
48 Crystalline Nanodroplets. *Phys. Rev. Lett.* **2010**, *105*, 237801-237804.
49
50
51
52
53
54
55
56
57
58
59
60

17. Weber, C. H. M.; Chinche, A.; Krausch, G.; Rosenfeldt, S.; Ballauff, M.; Harnau, L.; Göttker-Schnetmann, I.; Tong, Q.; Mecking, S. Single Lamella Nanoparticles of Polyethylene. *Nano Lett.* **2007**, *7*, 2024-2029.
18. Frank, C. W.; Rao, V.; Despotopoulou, M. M.; Pease, R. F. W.; Hinsberg, W. D.; Miller, R. D.; Rabolt, J. F. Structure in thin and ultrathin spin-cast polymer films. *Science* **1996**, *273*, 912-915.
19. Kumaki, J.; Kawauchi, T.; Yashima, E. Two-Dimensional Folded Chain Crystals of a Synthetic Polymer in a Langmuir - Blodgett Film. *J. Am. Chem. Soc.* **2005**, *127*, 5788-5789.
20. Ma, Y.; Hu, W.; Reiter, G. Lamellar Crystal Orientations Biased by Crystallization Kinetics in Polymer Thin Films. *Macromolecules* **2006**, *39*, 5159-5164.
21. Toolan, D. T. W.; Isakova, A.; Hodgkinson, R.; Reeves-McLaren, N.; Hammond, O.; Edler, K. J.; Briscoe, W. H.; Arnold, T.; Gough, T.; Topham, P. D.; Howse, J. R. Insights into the Influence of Solvent Polarity on the Crystallization of Poly(ethylene oxide) Spin-Coated Thin Films via in Situ Grazing Incidence Wide-Angle X - ray Scattering. *Macromolecules* **2016**, *49*, 4579-4586.
22. Aissou, K.; Kwon, W.; Mumtaz, M.; Antoine, S.; Maret, M.; Portale, G.; Fleury, G.; Hadziioannou, G. Archimedean Tilings and Hierarchical Lamellar Morphology Formed by Semicrystalline Miktoarm Star Terpolymer Thin Films. *ACS Nano* **2016**, *10*, 4055-4061.
23. Bisbey, R. P.; DeBlase, C. R.; Smith, B. J.; Dichtel, W. R. Two-dimensional Covalent Organic Framework Thin Films Grown in Flow. *J. Am. Chem. Soc.* **2016**, *138*, 11433-11436.

24. Reiter, G.; Sommer, J. Crystallization of Adsorbed Polymer Monolayers. *Phys. Rev. Lett.* **1998**, *80*, 3771-3774.
25. Karki, A.; Nguyen, L.; Sharma, B.; Yan, Y.; Chen, W. Unusual Morphologies of Poly(vinyl alcohol) Thin Films Adsorbed on Poly(dimethylsiloxane) Substrates. *Langmuir* **2016**, *32*, 3191-3198.
26. Xu, J.; Chen, T.; Yang, C.; Li, Z.; Mao, Y.; Zeng, B.; Hsiao, B. S. Isothermal Crystallization of Poly(L -lactide) Induced by Graphene Nanosheets and Carbon Nanotubes: A Comparative Study. *Macromolecules* **2010**, *43*, 5000-5008.
27. Laird, E. D.; Wang, W.; Cheng, S.; Li, B.; Presser, V.; Dyatkin, B.; Gogotsi, Y.; Li, C. Y. Polymer Single Crystal-Decorated Superhydrophobic Buckypaper with Controlled Wetting and Conductivity. *ACS Nano* **2012**, *6*, 1204-1213.
28. Parros-Bujans, F.; Palomino, P.; Fernandez-Alonso, F.; Rudic, S.; Alegria, A.; Colmenero, J.; Encisco, E. Intercalation and Con fi nement of Poly(ethylene oxide) in Porous Carbon Nanoparticles with Controlled Morphologies. *Macromolecules* **2014**, *47*, 8729-8737.
29. Prud'homme, R. E. Crystallization and morphology of ultrathin films of homopolymers and polymer blends. *Prog. Polym. Sci.* **2016**, *55-54*, 214-231.
30. Tol, R. T.; Mathot, V. B. F.; Reynaers, H.; Groeninckx, G. In *Relationship between Phase Morphology, Crystallization, and Semicrystalline Structure in Immiscible Polymer Blends*; Harrats, C., Thomas, S. and Groeninckx, G., Eds.; Micro- and nanostructured multiphase polymer blend systems: Phase Morphology and Interfaces; Taylor and Francis: Boca Raton, 2006; pp 391-420.

31. Kim, B.; Park, S. W.; Hammond, P. T. Hydrogen-Bonding Layer-by-Layer- Assembled Biodegradable Polymeric Micelles as Drug Delivery Vehicles from Surfaces. *ACS Nano* **2008**, *2*, 386-392.
32. Lei, Y.; Deng, P.; Lin, M.; Zheng, X.; Zhu, F.; Ong, B. S. Enhancing Crystalline Structural Orders of Polymer Semiconductors for Efficient Charge Transport via Polymer-Matrix-Mediated Molecular Self-Assembly. *Adv. Mater.* **2016**, *28*, 6687-6694.
33. Liu, Y.; Zhao, J.; Li, Z.; Mu, C.; Ma, W.; Hu, H.; Jiang, K.; Lin, H.; Ade, H.; Yan, H. Aggregation and morphology control enables multiple cases of high-efficiency polymer solar cells. *Nature Commun.* **2014**, *5*, 5293-1-8.
34. Pechkova, E.; Nicolini, C. Protein nanocrystallography: a new approach to structural proteomics. *Trends Biotechnol.* **2004**, *22*, 117-122.
35. Chen, C.; Zuckermann, R. N.; DeYreo, J. J. Surface-Directed Assembly of Sequence-Defined Synthetic Polymers into Networks of Hexagonally Patterned Nanoribbons with Controlled Functionalities. *ACS Nano* **2016**, *10*, 5314-5320.
36. Gulde, M.; Rissanou, A. N.; Harmandaris, V.; Müller, M.; Schäfer, S.; Ropers, C. Dynamics and Structure of Monolayer Polymer Crystallites on Graphene. *Nano Lett.* **2016**, *16*, 6994-7000.
37. Gulde, M.; Schweda, S.; Storeck, G.; Maiti, M.; Hak Ki, Y.; Wodtke, A. M.; Schäfer, S.; Ropers, C. Ultrafast low-energy electron diffraction in transmission resolves polymer/ graphene superstructure dynamics. *Science* **2014**, *345*, 200-204.

38. Chundawat, S. P. S.; Bellesia, G.; Uppugundla, N.; da Costa Sousa, L.; Gao, D.; Cheh, A. M.; Agarwal, U. P.; Bianchetti, C. M.; Phillips, G. N. J.; Langan, P.; Balan, V.; Gnanakaran, S.; Dale, B. E. Restructuring the Crystalline Cellulose Hydrogen Bond Network Enhances Its Depolymerization Rate. *J. Am. Chem. Soc.* **2011**, *133*, 11163-11174.
39. Wada, M.; Chanzy, H.; Nishiyama, Y.; Langan, P. Cellulose III_I Crystal Structure and Hydrogen Bonding by Synchrotron X-ray and Neutron Fiber Diffraction. *Macromolecules* **2004**, *37*, 8548-8555.
40. Parthasarathi, R.; Bellesia, G.; Chundawat, S. P. S.; Dale, B. E.; Langan, P.; Gnanakaran, S. Insights into Hydrogen Bonding and Stacking Interactions in Cellulose. *J. Phys. Chem. A* **2011**, *115*, 14191-14202.
41. Wada, M.; Heux, L.; Isogai, A.; Nishiyama, Y.; Chanzy, H.; Sugiyama, J. Improved Structural Data of Cellulose III_I Prepared in Supercritical Ammonia. *Macromolecules* **2001**, *34*, 1237-1243.
42. Wada, M.; Kwon, G. J.; Nishiyama, Y. Structure and Thermal Behavior of a Cellulose I-Ethylenediamine Complex. *Biomacromolecules* **2008**, *9*, 2898-2904.
43. Lokhande, H. T.; Shukla, S. R.; Chidambareswaran, P. K.; Patil, N. B. Ethylenediamine-induced conversion of cellulose I to cellulose III. *J. Polym. Sci. Polym. Lett. Ed.* **1977**, *15*, 97-99.
44. Roche, E.; Chanzy, H. Electron microscopy study of the transformation of cellulose I into cellulose III_I in *Valonia*. *Int. J. Biol. Macromol.* **1981**, *3*, 1981-206.

45. Chen, P.; Marianski, M.; Baldauf, C. H-Bond Isomerization in Crystalline Cellulose III: Proton Hopping versus Hydroxyl Flip-Flop. *ACS Macro Lett.* **2016**, *5*, 50-54.
46. Ono, Y.; Tanaka, R.; Funahashi, R.; Takeuchi, M.; Saito, T.; Isogai, A. SEC-MALLS analysis of ethylenediamine-pretreated native celluloses in LiCl/N,N-dimethylacetamide: softwood kraft pulp and highly crystalline bacterial, tunicate, and algal celluloses. *Cellulose* **2016**, *23*, 1639-1647.
47. Edgar, C. D.; Gray, D. G. Smooth model cellulose I surfaces from nanocrystal suspensions. *Cellulose* **2003**, *10*, 299-306.
48. Beck, S.; Bouchard, J.; Berry, R. Dispersibility in Water of Dried Nanocrystalline Cellulose. *Biomacromolecules* **2012**, *13*, 1486-1494.
49. Labet, M.; Thielemans, W. Improving the reproducibility of chemical reactions on the surface of cellulose nanocrystals: ROP of ϵ -caprolactone as a case study. *Cellulose* **2011**, *18*, 607-617.
50. Ahola, S.; Salmi, J.; Johansson, L.; Laine, J.; Österberg, M. Model films from native cellulose nanofibrils. Preparation, swelling, and surface interactions. *Biomacromolecules* **2008**, *9*, 1273-1282.
51. van Duffel, B.; Verbiest, T.; Van Elshocht, S.; Persoons, A.; De Schryver, F. C.; Schoonheydt, R. A. Fuzzy Assembly and Second Harmonic Generation of Clay/Polymer/Dye Monolayer Films. *Langmuir* **2001**, *17*, 1243-1249.

52. Chanzy, H.; Henrissat, B.; Vincendon, M.; Tanner, S. F.; Belton, P. S. Solid-state ^{13}C -N.M.R. and electron microscopy study on the reversible cellulose I \rightarrow III $_I$ transformation in *Valonia*. *Carbohydr. Res.* **1987**, *160*, 1-11.
53. Isogai, A.; Usuda, M.; Kato, T.; Toshiyuki, U.; Atalla, R. H. Solid-state CP/MAS ^{13}C NMR Study of Cellulose Polymorphs. *Macromolecules* **1989**, *22*, 3168-3172.
54. Brinkmann, A.; Chen, M.; Couillard, M.; Jakubek, Z. J.; Leng, T.; Johnston, L. J. Correlating Cellulose Nanocrystal Particle Size and Surface Area. *Langmuir* **2016**, *32*, 6105-6114.
55. Jin, E.; Guo, J.; Yang, F.; Zhu, Y.; Song, J.; Jin, Y.; Rojas, O. On the polymorphic and morphological changes of cellulose nanocrystals (CNC-I) upon mercerization and conversion to CNC-II. *Carbohydr. Polym.* **2016**, *143*, 327-335.
56. Lokanathan, A.; Khan, M. A. U.; Rojas, O.; Laine, J. Cellulose nanocrystal-mediated synthesis of silver nanoparticles: role of sulfate groups in nucleation phenomena. *Biomacromolecules* **2014**, *15*, 373-9.
57. Elazzouzi-Harfaoui, S.; Nishiyama, Y.; Putaux, J. -L.; Heux, L.; Dubreuil, F.; Rochas, C. The Shape and Size Distribution of Crystalline Nanoparticles Prepared by Acid Hydrolysis of Native Cellulose. *Biomacromolecules* **2008**, *9*, 57-65.
58. Nishiyama, Y.; Sugiyama, J.; Chanzy, H.; Langan, P. Crystal Structure and Hydrogen Bonding System in Cellulose I $_{\alpha}$ from Synchrotron X-ray and Neutron Fiber Diffraction. *J. Am. Chem. Soc.* **2003**, *125*, 14300-14306.
59. Geim, A. K.; Grigorieva, I. V. Van der Waals heterostructures. *Nature* **2013**, *499*, 419-425.

60. Bhimanapati, G. R.; Lin, Z.; Meunier, V.; Jung, Y.; Cha, J.; Das, S.; Xiao, D.; Son, Y.; Strano, M. S.; Cooper, V. R.; Liang, L.; Louie, S. G.; Ringe, E.; Zhou, W.; Kim, S. S.; Naik, R. R.; Sumpter, B. G.; Terrones, H.; Xia, F.; Wang, Y.; Zhu, J.; Akinwande, D.; Alem, N.; Schuller, J. A.; Schaak, R. E.; Terrones, M.; Robinson, J. A. Recent Advances in Two-Dimensional Materials beyond Graphene. *ACS Nano* **2015**, *9*, 11509-11539.
61. Novoselov, K. S.; Geim, A. K.; Morozov, S. V.; Jiang, D.; Zhang, Y.; Dubonos, I. V.; Firsov, A. A. Electric Field Effect in Atomically Thin Carbon Films. *Science* **2004**, *306*, 666-669.
62. Lebedeva, N. V.; Sun, F. C.; Lee, H.; Matyjaszewski, K.; Sheiko, S. S. "Fatal Adsorption" of Brushlike Macromolecules: High Sensitivity of C–C Bond Cleavage Rates to Substrate Surface Energy. *J. Am. Chem. Soc.* **2008**, *130*, 4228-4229.
63. Li, Q.; Renneckar, S. Supramolecular Structure Characterization of Molecularly Thin Cellulose I Nanoparticles. *Biomacromolecules* **2011**, *12*, 650-659.

Table of Contents Graphics

